Hybrid Quantum Classical Molecular Dynamics Simulation of the Proton-Transfer Reaction of HO^- with HBr in Aqueous Clusters

M. Dolores Elola and Dario A. Estrin*

Departamento de Química Inorgánica, Analítica y Química Física, and Inquimae, Facultad de Ciencias Exactas y Naturales, Universidad de Buenos Aires, Ciudad Universitaria, Pabellón 2, 1428, Buenos Aires, Argentina

Daniel Laria

Unidad de Actividad Química, Comisión Nacional de Energía Atómica, Avenida del Libertador 8250, 1429, Buenos Aires, Argentina, and Departamento de Química Inorgánica, Analítica y Química Física and Inquimae, Facultad de Ciencias Exactas y Naturales, Universidad de Buenos Aires, Ciudad Universitaria, Pabellón 2, 1428, Buenos Aires, Argentina

Received: September 11, 1998; In Final Form: December 7, 1998

A hybrid quantum classical computational algorithm, which couples a density functional Hamiltonian to a classical bath, is applied to investigate the proton-transfer reaction $OH^- + HBr \rightarrow H_2O + Br^-$ in aqueous clusters. The reagent was modeled using density functional theory with a Gaussian basis set; two different force fields for the classical bath were investigated: the TIP4P-FQ fluctuating charge and the TIP4P mean field potentials. Basis sets, functionals, and force field parameters have been validated by performing calculations on $[HO^-](H_2O)$, $[Br^-](H_2O)$, $[HBr](H_2O)$, and $[H_2O](H_2O)$ isolated dimers at 0 K. Molecular dynamics simulations of the system $[HOHBr]^-(H_2O)_n$, with $n = 2$ and 6, show that the reaction is spontaneous and rather exothermic, leading to the full detachment of the bromide ion from the halide and the generation of a water molecule within a few femtoseconds. In addition, our experiments show that the process involves a fast damping of the potential energy concomitant with a sudden increase of the vibrational kinetic energy of the newly formed HO bond in the water molecule. The gradual dissipation of the solute energy into the classical region led to an increase in the cluster sizes, suggesting the onset of cluster fragmentation; both phenomena evolve faster in the smallest clusters. The role of polarization effects in the classical subsystem on the reaction dynamics was also investigated by performing simulation experiments with the TIP4P potential. In these cases, the proton transfer is more exothermic, leading to fragmentation of the aggregates at earlier stages.

1. Introduction

Many chemical reactions take place under the influence of an environment or solvent. Since bond breaking and forming involved in reactive processes are inherently quantum mechanical in nature, empirical force fields used in classical simulation studies of solvated systems are not suitable to tackle this kind of processes in a realistic way. In a broad context, attempts to incorporate the effects of the environment within a quantum mechanical (QM) calculation can be classified into three main categories: (i) continuum solvation models, in which the solvent is replaced by a background characterized by a given set of macroscopic parameters, such as the bulk dielectric constant and/or a surface tension;[1,2] (ii) full ab initio QM calculations, where the whole system is treated quantum mechanically. Perhaps one of the most popular and successful schemes of this type of methods is the coupled density functional theory (DFT)−molecular dynamics approach proposed by Car and Parrinello[3−5] (iii) hybrid quantum classical mechanical (QM-CM) models.[6−10] The basic approximation of the latter methods involves partitioning the system under investigation into one subsystem that requires a rigorous QM treatment and an environment which is normally treated with empirical force fields. In addition to the lower computational costs when compared to a full QM calculation, these methods have also the advantage that they are based on concepts closely related to common chemical argumentation. Since the hybrid QM-CM idea was first proposed in 1976 by Warshel and Levitt,[6] a variety of models have been developed combining semiempirical,[6−8] Hartree−Fock,[9−11] and DFT[12,13] electronic structure methodologies with empirical force fields. Although most of the reported applications were devoted to solvation phenomena,[8,9,12] there have been several recent applications on chemical reactivity as well.[10,13−15]

A particularly interesting benchmark for testing hybrid QM-CM schemes consists of the investigation of chemical reactivity in aqueous clusters. In recent years, these systems have attracted the attention of many experimental[16−18] and theoretical [19−21] groups, due to the peculiar properties of the water substance and their relevance in atmospheric and environmental chemistry. In most of the currently employed hybrid schemes, the dynamics that governs the electronic charge distribution of the QM subsystem is performed within the adiabatic approximation, i.e., assuming an immediate adjustment of the electronic density of the quantum subsystem to the instantaneous ground-state potential energy surface generated by a given nuclear configuration. More refined models that take into account nonadiabatic transitions along the dynamics have also been proposed.[22,23]

10.1021/jp983678y CCC: $18.00
Published on Web 06/15/1999

Special caution should be exerted when one is interested in describing chemical reactions that take place in nanoaggregates. For such cases, the lack of translational symmetry along with the presence of a nearby free surface may also lead to considerable asymmetries in the local electric fields which, in turn, will be reflected in important polarization effects in the classical subsystem. The appropriate treatment of these effects usually requires the implementation of more elaborate descriptions of the Hamiltonian for the solvent beyond the usual mean field models. One such approach consists of the implementation of atom-centered induced point dipoles,[24,25] while another valid alternative makes use of the electronegativity equality principle[26,27] to derive fluctuating point charges on the CM interacting sites. These types of models have polarizabilities to all orders in the charge moments and are not restricted to a dipolar approximation. Moreover, the implementation of the latter scheme is straightforward in the context of hybrid QM-CM models since no new interactions are required.[28−30]

In this work, we report results of a molecular dynamics study of the proton-transfer reaction

$$HO^- + HBr \rightarrow H_2O + Br^- \qquad (1)$$

in small water clusters, using a Gaussian basis set DFT electronic structure methodology for the QM region and a polarizable Hamiltonian for the classical bath. The reaction has recently been investigated by Arnold et al.,[16] who have studied rate constants and fragmentation products for different cluster sizes. Arnold's experiments show a variety of products species and large variations in the reaction efficiency depending on the specific number of water molecules solvating the reagent; however, most of the experimental findings of the work were analyzed using enthalpic information, i.e., equilibrium energetic quantities. The present study represents a first attempt to incorporate, in an explicit fashion, the effects of spontaneous thermal and polarization fluctuations provided by different microenvironments that may be helpful to rationalize some experimental findings. It is well-known that in reactive processes involving a substantial reorganization of the electronic structure of the reagent such as charge-transfer reactions, the polar environment may induce important changes in the gas-phase reactive mechanisms.[31] For the sake of comparison, we have also performed several test runs using the nonpolarizable TIP4P[32] pseudopotential for the bath.

The organization of the paper is as follows: in section II we present a brief description of the model and the simulation method employed. Section III includes results for binding energies and geometrical parameters for selected quantum classical dimers at 0 K, including $[HO^-](H_2O)$, $[Br^-](H_2O)$, $[HBr](H_2O)$, and $[H_2O](H_2O)$. These preliminary runs were performed to validate the model and optimize different potential parameters. The results of the molecular dynamics experiments are shown in section IV; the conclusions of the work are presented in section V.

2. Model and Simulation Methods

Our molecular dynamics experiments were performed on a system containing a QM reactive complex $[HOHBr]^-$ and a CM subsystem composed of $n_w = 2$ and 6 water molecules. Consider a given configuration of n_w water molecules with atomic coordinates and partial charges $\{\mathbf{R}_{i\alpha}, q_{i\alpha}; i = 1, ..., n_w; \alpha = O, H, H\}$ and a set of atoms in the QM region with coordinates and nuclear charges $\{\tau_\alpha, z_\alpha; \alpha = Br, O, H, H\}$. We propose the following expression for the ground-state Born−Oppenheimer potential energy surface:

$$E[\{\mathbf{R}_{i\alpha}\}, \{\tau_\alpha\}; \rho] = E_{KS}[\rho] + E_{QM-CM} + E_{CM} \qquad (2)$$

where $E_{KS}[\rho]$ is a purely quantum mechanical piece given by the standard Kohn−Sham expression.[33] The second term E_{QM-CM} accounts for the coupling between the QM and CM subsystems and is given by

$$E_{QM-CM} = \sum_{i,\alpha} q_{i\alpha} \int \frac{\rho(\mathbf{r})}{|\mathbf{r} - \mathbf{R}_{i\alpha}|} d\mathbf{r} + \sum_{i,\alpha,\gamma} \left[\nu_{LJ}^{\alpha\gamma}(|\mathbf{R}_{i\alpha} - \tau_\gamma|) + \frac{q_{i\alpha} z_\gamma}{|\mathbf{R}_{i\alpha} - \tau_\gamma|} \right] \qquad (3)$$

The electronic density $\rho(\mathbf{r})$ was computed by solving a set of Kohn−Sham equations self-consistently at each step of the molecular dynamics run with an external potential contribution that includes the electrostatic interaction given in the first term of eq 3. The computation of the correlation portion was performed using the parametrization of the homogeneous electron gas of Vosko[34] and the gradient corrections derived by Lee, Yang, and Parr.[35] The local exchange term was supplemented with the gradient corrections proposed by Becke.[36] Both the exchange-correlation contribution to the Kohn−Sham potential and the electronic energy were calculated by a numerical integration scheme based on grids and quadratures also proposed by Becke.[37] Double-ζ plus polarization Gaussian basis sets were used for the expansion of the one-electron orbitals.[38] The electronic density was also expanded in an additional Gaussian basis set;[39] the coefficients for the fit of the electronic density were computed by minimizing the error in the Coulomb repulsion energy. The use of this procedure also results in an important speedup of the computations, since the cost of evaluating matrix elements is reduced from $O(N^4)$ to $O(N^2M)$ (N is the number of functions in the orbital set, and M the number of functions in the auxiliary set, typically of a size comparable to N). Auxiliary sets were also taken from ref 38.

The last term in the right-hand side of eq 3 corresponds to interactions between the nuclei in the CM and QM regions; they were modeled using a standard Lennard-Jones (6-12) term plus a purely Coulombic tail. E_{CM} in eq 2 represents the potential energy of the classical subsystem and was constructed using the TIP4P-FQ model proposed by Rick et al.[27] This model includes two contributions: the first one is a sum of site−site Lennard-Jones and Coulomb terms. The second term includes a quadratic expansion of the self-energy required to locate partial charges $\{q_{i\alpha}\}$ on the solvent sites.[27,40] Polarization effects are explicitly incorporated by allowing the partial charges to fluctuate along the simulation run. In principle, the instantaneous values of the set $\{q_{i\alpha}\}$ can be computed at each step using a variational principle. However, it is normally more efficient to generate the simultaneous time evolution of the spatial coordinates and the partial charges by considering the following extended Lagrangian:[27,41]

$$L = \frac{1}{2}\sum_\alpha M_\alpha \dot{\tau}_\alpha^2 + \frac{1}{2}\sum_{i,\alpha} M_\alpha \dot{\mathbf{R}}_{i\alpha}^2 + \frac{1}{2}\sum_{i\alpha} M_\alpha^q \dot{q}_{i\alpha}^2 - E[\{\mathbf{R}_{i\alpha}\}, \{q_{i\alpha}\}, \{\tau_\gamma\}; \rho] - \sum_{i,\alpha} \lambda_i q_{i\alpha} \qquad (4)$$

where M_α represents the mass of the αth atom, M_α^q is a fictitious mass associated to the dynamical variable $q_{i\alpha}$, and the set $\{\lambda_i\}$ corresponds to Lagrange multipliers of the con-

TABLE 1: Potential Parameters for the TIP4P, TIP4P−FQ Models and Lennard-Jones Parameters for QM Atoms; the Transfered Proton and the One in the Original HO^- Group are Denoted by H and H′, Respectively

parameter	TIP4P	TIP4P−FQ	H	Br	O	H′
ϵ^a (kJ/mol)	0.6485	1.1975	0.00	2.1532	1.1975	0.00
σ^a (Å)	3.154	3.159	0.00	4.233	3.159	0.00
q^b (e)	0.52	0.444	0.147	−0.147	−1.169	0.169

[a] The usual arithmetical and geometrical means were used to compute length and energy parameters for cross interactions. For the TIP4P and TIP4P−FQ models, the only nonzero σ_α and ϵ_α correspond to the oxygen site. [b] Partial charges on QM atoms were obtained from a DFT calculation of isolated HO^- and HBr.

TABLE 2. Binding Energies (kJ/mol) of Dimers

dimer	DFT-TIP4P	DFT-TIP4P-FQ	exptl	*ab initio*
$(H_2O)_2$[a]	−21.8	−21.1	−22.6 ± 2.9[c]	−20.6[d]
$(H_2O)_2$[b]	−23.1	−18.6	−22.6 ± 2.9[c]	−20.6[d]
$[HO^-](H_2O)$	−92.5	−161.3		−118.8[e]
$[HBr](H_2O)$	−20.9	−16.7		−17.3[f]
$[Br^-](H_2O)$	−42.2	−51.4	−49.0[g]	−46.3[h]

[a] Quantum water H-bond acceptor. [b] Quantum water H-bond donor. [c] Reference 46. [d] Reference 48. [e] Reference 50. [f] Reference 51. [g] Reference 52. [h] Reference 53.

straints associated to the electrical neutrality of the individual CM molecules. One important advantage of Rick et al.'s model is the fact that all the necessary derivatives in Newton's equations for the partial charges can be easily evaluated within the context of the hybrid DFT-CM scheme in terms of one-electron integrals.[42]

In all our simulation experiments, the Verlet algorithm[43] was employed to integrate Newton's equation of motion with a time step of 0.1 fs. All fictitious masses associated with charge dynamics were set to 6.0×10^{-5} kcal/mol (ps/e)^2. In addition, a Nosé thermostat set at 5 K was coupled to the partial charges in the TIP4P-FQ simulations to maintain the charge degrees of freedom decoupled from the nuclear motion.[27,41] Constraints associated with intramolecular distances in the water were treated using the SHAKE algorithm.[44] We have also performed a series of simulations using the nonpolarizable TIP4P model.[32] The geometry of the water molecule is identical to the polarizable model and there are slight changes in the values of the fixed charges and the LJ parameters. Full details of the length and energy parameters for both transferable potentials are given in Table 1.

3. Optimized Structures of Dimers

Before addressing the specific case of the proton-transfer reactions shown in eq 1 and in order to assess the quality of our approach, we performed a series of preliminary runs to compute the energetics and geometrical parameters of minimum energy configurations of some relevant quantum-classical model dimers. The results were obtained by successive quenchings of simulated structures using standard steepest descent procedures.[45] We started by considering two mixed quantum classical water dimers that differed in the role of the quantum water molecule as proton donor and acceptor, respectively.

In Tables 2, 3, and 4 we present results for the binding energies, the hydrogen bond distances, and partial charges in the classical water, respectively. For the sake of comparison, we have also included the experimental energetic results of Odutola et al.[46] and those obtained using more accurate treatments of the electronic structure.[47,48] When the classical water acts as proton donor, the explicit incorporation of site

TABLE 3. Optimized Bond Distances for Selected Dimers

dimer	DFT-TIP4P	DFT-TIP4P-FQ	exptl	ab initio
		d_{O-O} (Å)		
$(H_2O)_2$[a]	2.827	2.877	2.98[c]	2.913[d]
$(H_2O)_2$[b]	2.778	2.895	2.98[c]	2.913[d]
$[HO^-](H_2O)$	2.680	2.527		2.474[e]
		d_{O-Br} (Å)		
$[HBr](H_2O)$	3.434	3.512		3.496[f]
$[Br^-](H_2O)$	3.212	3.246		3.359[g]

[a] Quantum water H-bond acceptor [b] Quantum water H-bond donor [c] Reference 46. [d] Reference 48. [e] Reference 50. [f] Reference 51. [g] Full DFT calculation. This work.

TABLE 4: Partial Charges on Atoms (e) of Classical Water of Dimers

dimer	q_O	q_{H_1}[a]	q_{H_2}
$(H_2O)_2$[b]	−0.976	0.564	0.412
$(H_2O)_2$[c]	−0.975	0.4875	0.4875
$[HO^-](H_2O)$	−1.294	1.040	0.254
$[HBr](H_2O)$	−0.962	0.481	0.481
$[Br^-](H_2O)$	−1.062	0.702	0.360

[a] H_1 refers to the water hydrogen participating in the intramolecular bonding. [b] Quantum water H-bond acceptor. [c] Quantum water H-bond donor.

polarizabilities in the classical Hamiltonian leads to a considerable asymmetry in the charge populations of the hydrogen sites. The charge of the atom that participates in the hydrogen bond exhibits an increment of almost 25% above the usual mean field parametrization, $q_H \cong 0.42\ e$.[27] However, effects of asymmetry in the electronic distribution of the classical water seem to cancel out when one computes the binding energy for the dimer. Note that the resulting DFT-TIP4P-FQ binding energy $U_{TIP4P-FQ} = -21.1$ kJ mol^{-1} does not differ substantially from the mean field fixed charge DFT-TIP4P result $U_{TIP4P} = -21.8$ kJ/mol. Moreover, both are comparable to the experimental estimate $U_{exp} = -22.6 \pm 2.9$ kJ/mol.[46] For the bond distances d_{O-O}, we obtained 2.877 and 2.827 Å, for the calculations employing TIP4P−FQ and TIP4P potentials, respectively. Here again, both estimated values are comparable to the experimental result,[46] $d_{O-O} = 2.98$ Å, and to the results obtained using full ab-initio calculations.[47,48] For the reverse case, i.e., when the quantum water is the proton donor, the binding energy estimate for the DFT-TIP4P-FQ is somewhat less accurate $U_{TIP4P-FQ} = -18.6$ kJ/mol, while DFT-TIP4P calculations yield $U_{TIP4P} = -23.1$ kJ/mol. Since neither hydrogen atom of the classical molecule participates in the intramolecular bond, asymmetries in the charge distribution are less marked and we only found a small increase of about 0.07e in both atoms. The optimized d_{O-O} does not present important changes; we found 2.895 and 2.778 Å for the calculations employing TIP4P-FQ and TIP4P potentials for the classical water, respectively.

Another important dimer to be considered in the present context is the $[HO^-](H_2O)$ complex. For this case, calculations were performed assuming that the quantum subsystem was the hydroxyl anion and modeling the water molecule with both, TIP4P-FQ and TIP4P potentials. We found that the water molecule binds to the oxygen atom of the hydroxide anion forming an almost linear hydrogen bond in both calculations, an observation that is accordant to previous ab initio studies.[49,50] The optimized $d_{O-O} = 2.527$ Å for TIP4P-FQ agrees reasonably well with the ab initio result;[50] the fixed charge model yields a slightly overestimated value $d_{O-O} = 2.680$ Å. Considering now the predictions for the binding energy, the TIP4P result is −92.5 kJ/mol which is smaller than the ab initio MP2 result of −118.8

kJ/mol, while the TIP4P-FQ calculation overestimates this value yielding −161.3 kJ/mol. Consistently with this observation, large polarization effects take place in the TIP4P-FQ calculation. This is clearly reflected in the value of the charge of 1.04*e* on the classical proton that participates in the hydrogen bond.

For dimers involving a bromide atom, we have adjusted its Lennard-Jones length parameter in order to obtain the best agreement with experimental and ab initio results. The particular choice of this parameter usually requires a very careful tuning, especially in cases where the quantum subsystem is electrically nonneutral; under these circumstances, electronic density spill-out problems in the quantum subsystem are likely to appear if the Lennard-Jones parameter is inadequately chosen. We found good agreement with experiments and full ab initio calculations[51] by fixing $\sigma_{Br} = 4.233$ Å; for the case of the water−hydrogen bromide dimer, its geometry is predicted to be pyramidal with C_s symmetry. The agreement between the binding energies and the optimized d_{O-Br} obtained with both TIP4P models and the ab initio result is also reasonable being the TIP4P-FQ calculations somewhat closer to the full quantum result.

The last complex that we considered is the bromide−water dimer. In this case, results from DFT-TIP4P and DFT-TIP4P-FQ differ substantially: while the predicted optimized structure using the latter Hamiltonian presents an almost linear hydrogen bond with an angle of $\theta_{Br-H-O} = 171°$, the converged TIP4P calculation yields a structure with $\theta_{Br-H-O} = 137°$. We remark that the first spatial arrangement is much closer to the value $\theta_{Br-H-O} = 166°$ found in the full quantum DFT treatment. For this particular dimer, we confirmed that the lack of polarization on the TIP4P water molecules prevents a preferential binding between the quantum Br^- and one of the water hydrogens, which should be the correct minimum energy structure. Results for binding energies, geometrical parameters, and partial charges are also shown in Tables 2−4 where, for the sake of comparison, we also present experimental results[52] and predictions from ab initio calculations by Combariza et al.[53] as well. In all cases, the agreement between our hybrid QM-CM calculations using the TIP4P-FQ model and the results from previous studies is satisfactory.

4. Reaction Dynamics

Having established the performance of our hybrid scheme to predict minimum energy calculations for the most relevant complexes involved in the reactive process shown in eq 1, we now turn to its microscopic dynamical analysis. To that end, we started by performing a set of preliminary simulation experiments to generate initial conditions at $T \cong 200$ K using a simplified force field for the reactant species. In this scheme, HBr and OH^- were modeled as dipolar Lennard-Jones spheres centered at the O and Br atoms containing embedded atomic partial charges with the following charge separations: $d_{Br-H} = 1.434$ Å and $d_{O-H} = 0.996$ Å. Length and potential parameters for the solute−solvent potential for these preliminary runs are displayed in Table 1. At $t = 0$, the *classical* reagent was replaced by the quantum subsystem and we let the system evolve along microcanonical runs monitoring the time evolution of different parameters relevant to the reactive process for typical periods of 1 ps. To maintain better control on the kinetics of the fluctuating charges of the solvent, the Nosé thermostat was switched off during the initial 50 fs and successive rescalings of the charge velocities were performed every 0.5 fs. After that period, the Nosé thermostat was reinstalled. For each cluster size, we ran on the order of 10 different trajectories started from initial conditions separated by time intervals of the order of 5 ps to provide statistical independence. In all cases, we found that the characteristics of the nonequilibrium relaxations were practically the same.

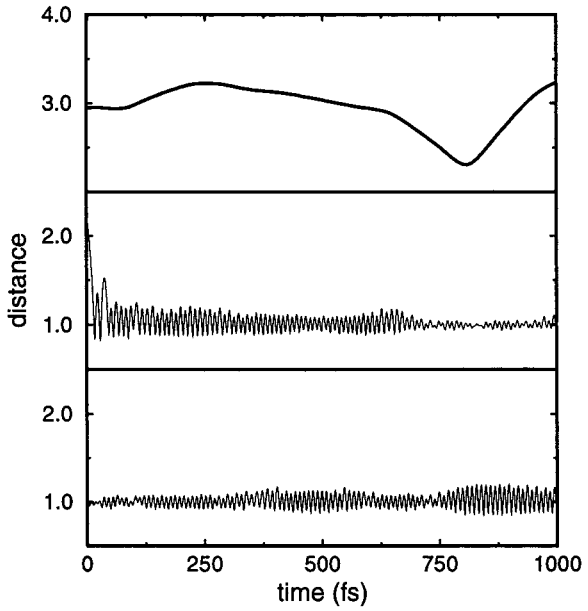

Figure 1. Time evolution of several length parameters (Å) for TIP4P-FQ clusters with $n_w = 2$ (see text): (top panel) d_{Br^--CM}; (center panel) d_{H-O}; (bottom panel) $d_{H'-O}$.

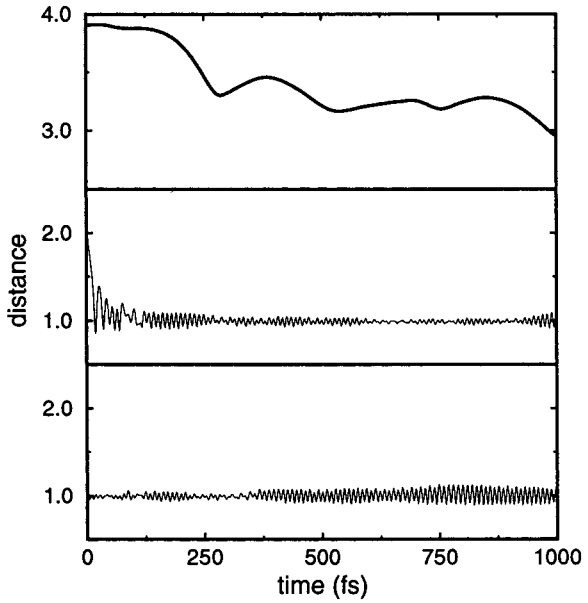

Figure 2. Same as Figure 1, for $n_w = 6$.

In Figures 1 and 2, we present results for the time evolution of different relevant distances $d_{\alpha-\gamma}$, for $[HOHBr]^-(H_2O)_n$ with $n_w = 2$ and 6, respectively, taken from a typical trajectory. For clarity purposes, it will be convenient to differentiate the transferred proton from the one in the original OH^- group by denoting the latter as H′. The almost immediate drop in d_{H-O} from approximately 2 Å down to values close to 1 Å depicted in the center panels clearly shows the immediate transfer of the proton from the Br to the OH^- group. For both cluster sizes, the initial excess potential energy is quickly redistributed within the different internal degrees of freedom of the new water molecule. This fact is reflected in the growing size of the fluctuations in $d_{O-H'}$ shown in the bottom panels; after $t \approx 50$

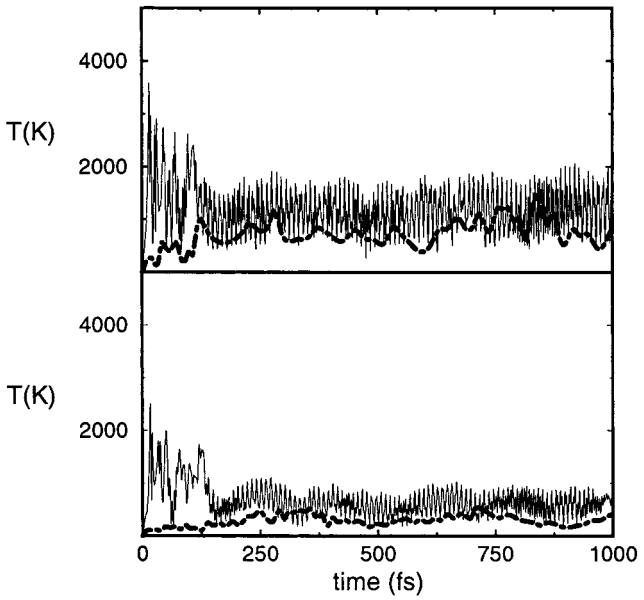

Figure 3. Temperatures for quantum and classical subsystems as a function of time for $[HOHBr]^-(H_2O)_2$ (top panel) and $[HOHBr]^-(H_2O)_6$ (lower panel). Results for the QM and CM subsystems are shown using solid and dashed lines, respectively.

fs for the $n_w = 2$ and $t \approx 370$ fs for the $n_w = 6$ cases, fluctuations in d_{O-H} and $d_{O-H'}$ become comparable. Moreover, note that even after 1 ps, the overall vibrational dynamics still looks rather asymmetric with larger fluctuations in $d_{O-H'}$ than in d_{O-H}. To investigate the solvation structure of the newly formed Br^- within the clusters, in the top panels we present the time evolution of $d_{Br^- - CM}$, the distance between the ion and the center of mass of the water molecules. After the transfer takes place, the inspection of several cluster configurations shows that the Br^- remains on the cluster surface solvated by a variable number of water molecules. It is also clear that after $t = 200$ fs, $d_{Br^- - CM}$ seems to be equilibrated at typical values that are comparable with the linear dimensions of the clusters.

As the reaction proceeds, the large acceleration of the transferred proton leads to a significant increase of the overall kinetic energy of the aggregates. The time evolution of the nuclear temperatures for the quantum and classical subsystems is shown in Figure 3. Note that, during the initial 5−10 fs, the temperature of quantum nuclei raises up to $T \approx 2000-3500$ K, depending on the cluster size, and that, after this initial stage, the kinetic energy of the quantum subsystem presents fast oscillations with typical periods of 10−12 fs. This period is comparable to those found in the time evolution of the two OH stretches shown in Figures 1 and 2, suggesting a markedly vibrational character of the nuclear kinetics of the quantum subsystem with a much smaller contribution from translational or rotational modes of the Br^- and the H_2O molecule.

The subsequent dissipation of the excess of thermal energy initially deposited in the solute into the classical bath is a much slower process.[54] To provide some estimative idea for the rate on the kinetic energy transfer, the smallest classical subsystem required of the order of half a picosecond to reach $T \approx 800$ K. Yet, note that after 1 ps the differences in temperature between the quantum and classical systems are still such that the cluster is far from having reached a thermally equilibrated state. Of course, for the largest clusters, a similar amount of dissipated energy gives rise to a more moderate heating of the classical bath since the number of available degrees of freedom is larger. With these observations in mind, one could wonder whether

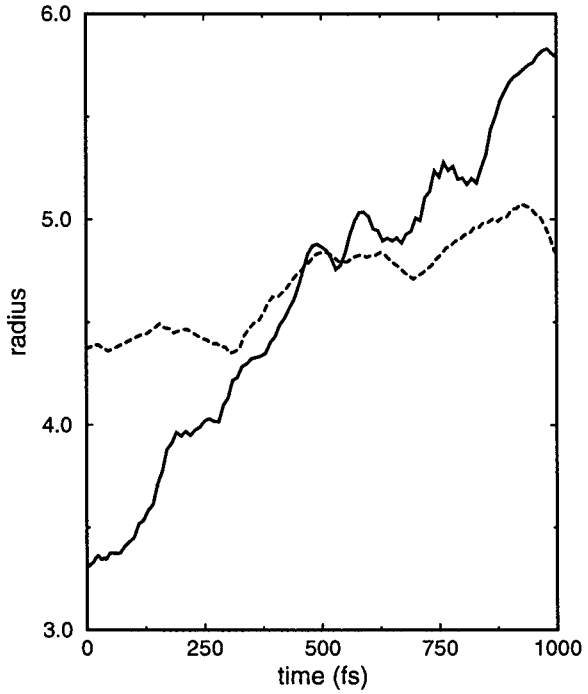

Figure 4. Gyration radius (Å) as a function of time for $[HOHBr]^-(H_2O)_2$ (solid lines) and $[HOHBr]^-(H_2O)_6$ (dashed lines).

these considerable increments in the overall kinetic energy would lead to the spontaneous fragmentation of the cluster, as it is found in real experiments,[16] in the time scales of our simulations. Changes in cluster linear dimensions can be conveniently monitored by inspecting the cluster gyration radius R, defined as

$$R^2 = \frac{1}{2N_n^2} \sum_{\alpha,\gamma} |\mathbf{r}_\alpha - \mathbf{r}_\gamma|^2 \tag{5}$$

where $\mathbf{r}_\alpha$ denotes the position of the α-th nucleus and N_n represents the total number of nuclei. Results for R are shown in Figure 4. For $n_w = 2$, there is a steady growth in the magnitude of R which clearly preannounces the forthcoming cluster fragmentation. For $n_w = 6$, the raise in R was found to be a much slower process, a result that is accordant to the slower rate of energy transfer mentioned in the previous paragraph (cf Figure 3).

The final aspect that we have investigated is related to the dynamics of the solvation response of the classical water environments. The most direct route to characterize the dynamics of the surrounding that follows the proton-transfer reaction is by inspecting the normalized relaxation of the coupling $S(t)$ defined as

$$S(t) = \frac{V_c(t)}{V_c(0)} \tag{6}$$

where $V_c(t)$ represents the Coulomb portion of the potential energy between the classical and quantum subsystems at time t.[55] A rigorous treatment of the cluster response $S(t)$ would require an average of the coupling $V_c(t)$ taken from an ensemble of trajectories started at different nonequilibrium initial conditions.[56] However, we believe that it is more instructive to present here the analysis of just a single trajectory trying to establish a correspondence between the most important features of $S(t)$ and specific details of the transient of the solvation structures. Note

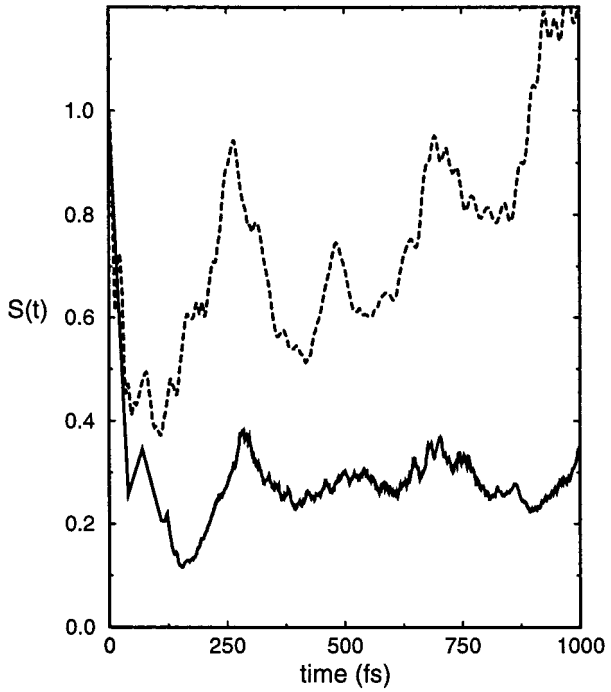

Figure 5. Normalized time relaxation of the solute−solvent electrostatic coupling for $n_w = 6$ clusters. The solid and dashed lines correspond to the TIP4P-FQ and TIP4P Hamiltonians, respectively.

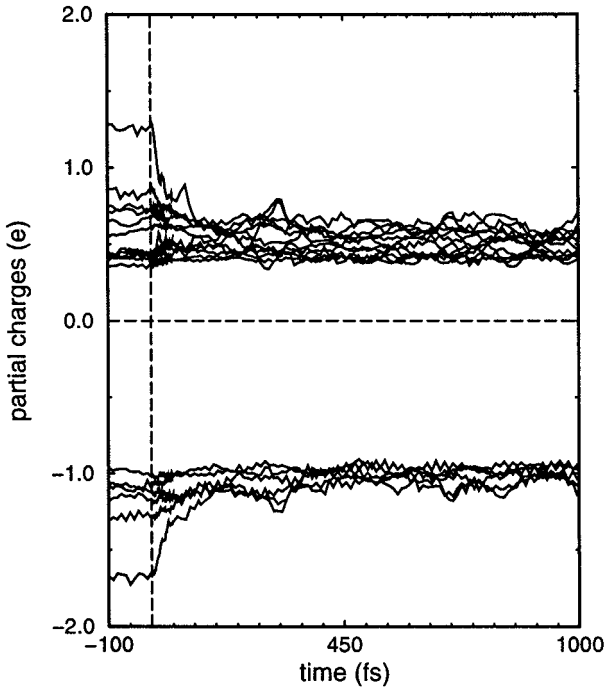

Figure 6. Time evolution of the partial charges on a $n_w = 6$ TIP4P-FQ water cluster: (top panel) hydrogen atoms; (lower panel) oxygen atoms.

that many of the observations that will follow in the next paragraphs would have been obscured if we had chosen to present results for a nonequilibrium average of $S(t)$.

Figure 5 shows results for $S(t)$ for the $n_w = 6$ cluster. Practically 80% of the bath response is completed after the initial $\Delta t \approx 100$ fs. Considering the magnitude of the gap in the coupling, the drop of $S(t)$ can be easily rationalized by simply inspecting the differences between the binding energies shown in Table 2 for the dimers $[OH^-](H_2O)$, which contributes to a large extent to the complex−solvent potential Coulombic energy at $t = 0$, and $[Br^-](H_2O)$, which provides the most important Coulomb contribution after the transfer takes places. During the early stages of the relaxation, the classical bath can respond using, at least, two main mechanisms. The first one consists of modifying its polarization. The fictitious masses associated to the set $\{q_i(t)\}$ were chosen sufficiently light to allow an almost instantaneous adjustment of the molecular polarizations to the characteristics of the rapidly changing local electric fields generated by the solute. In addition, the solvent molecules can modify their orientation and their positions within the clusters. However, one must keep in mind that the correct interpretation of the solvation response of most polar environments usually requires a collective interpretation of the phenomenon.[57] Consequently, the distinction between charge and rotational dynamical contributions is somewhat artificial since, in fact, both effects are very much interconnected. Anyhow, given the fast relaxation time scale found in our experiments (of the order of 100 fs), we can safely discard any major contributions arising from translational modes since, during such a period, the molecules remain practically at the same positions.

In Figure 6, we present a complementary prospective of the dynamical solvation response of an $n_w = 6$ cluster as it is reflected by the time dependence of the fluctuating charges of the individual water molecules. In the graph, we have also included a negative portion of the x axis that corresponds to the time evolution of the charges during the preliminary equilibration run. Two important aspects of this figure are worth commenting on. (i) The first is the large disparity that exists between the polarization of one particular water molecule and the rest of the bath, during negative times. A careful inspection of several snapshots of cluster configurations during this period reveals that the singular water molecule corresponds to the one that is initially hydrogen bonded to the OH^- group. This molecule exhibits partial charges $q_O \approx -1.7e$ and $q_H \approx 1.3e$ for the hydrogen that is bonded to the OH^- group. (ii) Once the complex is allowed to react, the initial asymmetries in the charge distribution of the solvent molecules disappear after 100 fs, a period comparable to that of the decay of $S(t)$. The simple consideration of the larger size of the Br^-, compared to the OH^-, is sufficient to explain the absence of any unusually large polarization of solvent molecules in the vicinity of the ion. Again, given the similarity in time scales, one could be tempted to ascribe the initial portion of the relaxation of $S(t)$ to the dynamics of the partial charges. However, this assertion is not totally valid since rotational relaxation of water molecules normally requires similar time scales as those found here.[57,58]

As a final comparative test, we have performed a few runs using the nonpolarizable TIP4P model. Interestingly, in these aggregates, once the transfer took place, we found that the quantum water remained mostly segregated from the rest of the cluster and normally got expelled after a few hundreds of femtoseconds. One partial explanation for this observation could be found in the fact that, in reality, the quantum water behaves very differently from the rest of the classical molecules. Again, a simple analysis based on the comparison between binding energies for different dimers can be helpful to make this point even more clear; note that the entries of Table 2 show that both mixed TIP4P−quantum water dimers are less stable than a pair of TIP4P molecules ($U_{TIP4P} = -26.0$ kJ/mol). Consequently, we tend to believe that, at least from an energetic point of view, the intramolecular connectivity of our quantum water is quite different from the rest. We remark that a major advantage of the polarizable model is the fact that these differences are much less marked; the binding energy of a pair of classical polarizable

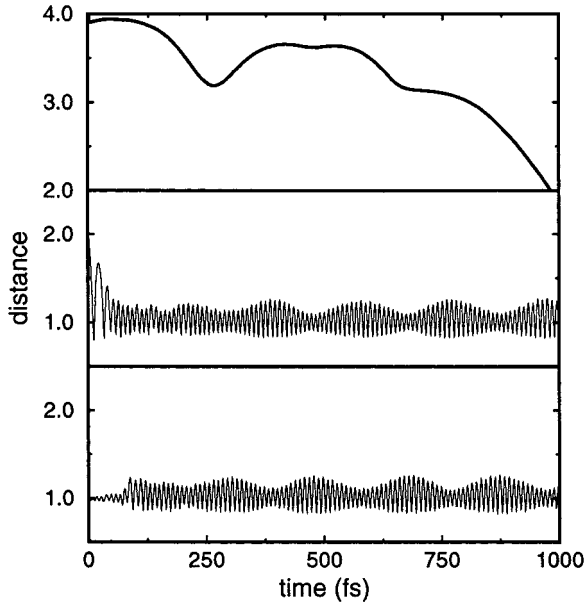

Figure 7. Same as Figure 2, for the TIP4P potential.

waters, $U_{TIP4P-FQ} = -18.8$ kJ/mol, is intermediate between the two values of hybrid quantum classical pairs shown in Table 2.

Results for the relaxation of the solute−solvent Coulomb coupling and relevant distances for an $n_w = 6$ TIP4P cluster are shown in Figures 5 and 7. Although the initial drop of $S(t)$ involves a similar time scale (≈100 fs), its magnitude is approximately half of that found for the polarizable model. To explain this observation, one should consider that, during this short period, the changes in Coulomb solute−solvent coupling are essentially due to the difference between the binding energies of the ionic dimers present in products and reactant states, namely, $[Br^-](H_2O)$ and $[HO^-](H_2O)$, respectively. This difference is of the order of 50 kJ/mol, a value that practically matches half of that found for the polarizable Hamiltonian. Another equivalent manifestation of the disparity in the dimer binding energies is reflected in the much larger fluctuations found in the two OH bond distances of the quantum water (see Figure 7). We believe that this is due to two main reasons: first, the larger net energy release during the transfer, and second, the fact that the quantum water gets segregated from the cluster, preventing the energy flow from the vibrational modes to the rest of the degrees of freedom. We conclude our analysis with a final comment on the time evolution of d_{Br^--CM}; the top panel of Figure 7 reveals that the bromide ion remains solvated by the classical nonpolarizable particles. Moreover, d_{Br^--CM} decreases during the final portion of the trajectory, a fact that could be indicative of the occurrence of *bulklike* solvation. The inspection of several cluster configurations reveals that this is partially true since the decrease in d_{Br^--CM} is also related to the much more compact structures found in TIP4P clusters. Under these circumstances, all relevant length scales would tend to be smaller. Additional evidence of the alternation between *bulklike* and superficial solvation can also be found in the much more pronounced oscillations exhibited by $S(t)$; we have verified that the maxima at 264, 700, and 980 fs can be correlated with *bulklike* states that exhibit larger ionic coordination numbers than superficial ones.

5. Concluding Remarks

In this study, we have presented the implementation of a hybrid quantum classical computational scheme that is able to capture many important features that characterize the dynamics of a model proton-transfer reaction taking place in small water clusters. In particular, we have put special emphasis on determining the effects of the microenvironment on the reactive mechanisms. To that end, we have considered two Hamiltonians with well differentiated polarization responses. Special attention was given to incorporating two important ingredients that we believe should be present in any realistic representation of a charge-transfer process in clusters: (i) a rigorous treatment of the rearrangement of the reagent electronic structure using accurate DFT calculations; (ii) an explicit incorporation of polarization effects on the classical bath via a Hamiltonian with time dependent fluctuating charges. The latter represents an essential element that cannot be neglected, especially in cases, as in the present one, where the environment in the closest vicinity of the reactant is affected by large fluctuations in the magnitude of the local electric fields. The magnitude of these fluctuations is even more pronounced in cluster environments due to the inhomogeneities in the spatial distribution of the molecules and the presence of a nearby free boundary.

From a computational point of view, an important advantage of the method presented here is the fact that the algorithm has proved to be sufficiently robust to provide stable results and reasonable energy conservation during several picoseconds without any further special care besides proper thermalization of the solvent fluctuating charges during the first initial period. The model reaction considered in this study represents a severe test for the algorithm since, during the proton transfer, kinetic and potential energies present changes well beyond the size of the spontaneous thermal fluctuations that take place during the previous classical equilibration run.

Of course, the description that we have presented here is far from being complete, and still there are some important questions that remain to be answered. For example, in our treatment, we have neglected nuclear quantum fluctuations. We could have employed a path integral scheme to treat both electronic structure and quantum nuclear fluctuations;[59] however, these techniques do not yield information about the dynamics of the process. Moreover, since the proton transfer considered in this work presents no barriers, we believe that zero-point energy and quantum tunneling effects should be negligible. A more delicate aspect that would merit further investigation is to evaluate the effects of incorporating additional water molecules into the quantum subsystem. More specifically, one could speculate on the relevance of alternative reaction paths in aqueous clusters such as the following double proton transfer, bridged by a second water molecule,

$$HBr + H_2O \rightarrow Br^- + H_3O^+$$

$$H_3O^+ + OH^- \rightarrow 2H_2O \qquad (7)$$

as a possible indirect reaction path. Moreover, should this process become thermodynamically possible, it would be important to determine whether the double transfer takes place in a concerted or sequential fashion. Although a detailed microscopic analysis of mechanisms such as the one proposed in eq 7 is beyond the scope of this study, its simple consideration underlines the importance of exploring the relevance of different reactive channels in clusters that perhaps are excluded in more conventional bulk phases.

Acknowledgment. D.L. and D.A.E. are members of the Carrera del Investigador Científico del CONICET (Argentina).

Partial economic support from the University of Buenos Aires, CONICET, and Fundación Antorchas of Argentina is very much appreciated. D.L. and D.A.E. thank the ICTP (Trieste, Italy) for hospitality.

References and Notes

(1) Cramer, C. J.; Truhlar, D. G. in *Solvent Effects and Chemical Reactivity*; Tapia, O., Ed.; Kluwer Academic Publishers: Dordrecht, 1996.
(2) Li, J.; Hawkins, G. D.; Cramer, C. J.; Truhlar, D. G. *Chem. Phys. Lett.* **1998**, *288*, 293.
(3) Car, R.; Parinello, M. *Phys. Rev. Lett.* **1985**, *55*, 2471.
(4) Meijer, E. J.; Sprik, M. *J. Phys. Chem. A* **1998**, *102*, 2893.
(5) Tuckerman, M.; Laasonen, K.; Sprik, M.; Parrinello, M. *J. Phys. Chem.* **1995**, *99*, 5749.
(6) Warshel, A.; Levitt, M. *J. Mol. Biol.* **1976**, *103*, 227.
(7) Field, M. J.; Bash, P. A.; Karplus, M. *J. Comput. Chem.* **1990**, *11*, 700.
(8) Gao, J. *J. Phys. Chem* **1992**, *96*, 6432.
(9) Stanton, R. V.; Little, L. R.; Merz, K. M. *J. Phys. Chem* **1995**, *99*, 17344.
(10) Singh, U. C.; Kollman, P. A. *J. Comput. Chem.* **1986**, *7*, 718.
(11) Estrin, D. A.; Liu, L.; Singer, S. J. *J. Phys. Chem.* **1992**, *96*, 5325.
(12) Stanton, R. V.; Hartsough, D. S.; Merz, K. M. *J. Phys. Chem.* **1993**, *97*, 11868.
(13) Estrin, D. A.; Kohanoff, J.; Laria, D. H.; Weht, R. O. *Chem. Phys. Lett.* **1997**, *280*, 280.
(14) Hartsough, D.; Merz, K. M. *J. Phys. Chem.* **1995**, *99*, 11266.
(15) (a) Tuñón, I.; Martins-Costa, M. T. C.; Millot, C.; Ruiz-lópez, M. F. *J. Chem. Phys.* **1997**, *106*, 3633. (b) Strnad, M.; Martins-Costa, M. T. C.; Millot, C.; Tuñón, I.; Ruiz-López, M. F.; Rivail, J. L. *J. Chem. Phys.* **1997**, *106*, 3643.
(16) Arnold, S. T.; Viggiano, A. A. *J. Phys. Chem. A* **1997**, *101*, 2859.
(17) Wincel, H.; Mereand, E.; Castleman, A. W. *J. Phys. Chem. A* **1997**, *101*, 8248.
(18) Seeley, J. V.; Morris, R. A.; Viggiano, A. A. *J. Phys. Chem.* **1996**, *100*, 15821.
(19) Re, M.; Laria, D. *J. Chem. Phys.* **1996**, *105*, 4589.
(20) For a recent review of the present advances in the area, see, for example: *Reaction Dynamics in Clusters and Condensed Phases*; Jortner, J., Levine, R. D., Pullman, B., Eds.; Kluwer: Dordrecht, 1994.
(21) Constas, S.; Kapral, R. *J. Chem. Phys.* **1994**, *101*, 10908; **1996**, *104*, 4581.
(22) Tully, J. C. *J. Chem. Phys.* **1990**, *93*, 1061.
(23) Coker, D. F. In *Computer Simulation in Chemical Physics*; Allen, M. P., Tildesley, D. J., Eds.; Kluwer Academic Publishers: Dordrecht, 1997; p 315.
(24) Thompson, M. A. *J. Phys. Chem.* **1996**, *100*, 14492.
(25) Bakowies, D.; Thiel, W. *J. Phys. Chem.* **1996**, *100*, 10580.
(26) Rappé, A. K.; Goddard, W. A. *Mol. Phys.* **1991**, *95*, 3358.
(27) Rick, S. W.; Stuart, S. J.; Berne, B. J. *J. Chem. Phys.* **1994**, *101*, 6141.
(28) Field, M. J. *Mol. Phys.* **1997**, *91*, 835.
(29) Bryce, R. A.; Buesnel, R.; Hillier, I. H.; Burton, N. A. *Chem. Phys. Lett.* **1997**, *279*, 367.
(30) Bryce, R. A.; Vincent, M. A.; Malcolm, N. O. J.; Hillier, I. H.; Burton, N. A. *J. Chem. Phys.* **1998**, *109*, 3077.
(31) See, for example: Hynes, J. T. In *Ultrafast Dynamics of Chemical Systems*; Simon, J. D., Ed.; Kluwer: Dordrecht, 1994; p 345.
(32) Jorgensen, W. L.; Chandrasekhar, J.; Madura, J. D.; Impey, R. W.; Klein, M. L. *J. Chem. Phys.* **1983**, *79*, 926.
(33) Kohn, W.; Sham, L. J. *Phys. Rev. A* **1965**, *140*, 1133.
(34) Vosko, S. H.; Wilk, L.; Nusair, M. *Can. J. Phys.* **1980**, *58*, 1200.
(35) Lee, C.; Yang, W.; Parr, R. *Phys. Rev. B* **1988**, *37*, 785.
(36) Becke, A. D. *Phys. Rev. A* **1988**, *38*, 3098.
(37) Becke, A. D. *J. Chem. Phys.* **1988**, *88*, 1053.
(38) Godbout, N.; Salahub, D. R.; Andzelm, J.; Wimmer, E. *Can. J. Chem.* **1992**, *70*, 560.
(39) Dunlap, B. I.; Connoly, J. W. D.; Sabin, J. R. *J. Chem. Phys.* **1979**, *71*, 3396; **1979**, *71*, 4993.
(40) Parr, R. G.; Yang, W. *Density Functional Theory of Atoms and Molecules;* Oxford University Press: New York, 1990.
(41) Sprik, M.; Klein, M. L. *J. Chem. Phys.* **1988**, *89*, 7556.
(42) Estrin, D. A.; Corongiu, G.; Clementi, E. In *METECC, Methods and Techniques in Computational Chemistry*; Clementi, E., Ed.; Stef: Cagliari, 1993; Chapter 12.
(43) Allen, M. P.; Tildesley, D. J. *Computer Simulations of Liquids*; Clarendon Press: Oxford, 1987.
(44) Ryckaert, J. P.; Ciccotti, G.; Berendsen, H. J. C. *J. Comput. Phys.* **1977**, *23*, 327.
(45) Press, W. H.; Flannery, B. P.; Teukolsky, S. A.; Vetterling, W. T. *Numerical Recipes*; Cambridge University Press: London, 1986.
(46) Odutola, J. A.; Dyke, T. R. *J. Chem. Phys.* **1980**, *72*, 6052.
(47) Estrin, D. A.; Paglieri, L.; Corongiu, G.; Clementi, E. *J. Phys. Chem.* **1996**, *100*, 8701.
(48) Hodges, M. P.; Stone, A. J.; Xantheas, S. S. *J. Phys. Chem. A* **1997**, *101*, 9163.
(49) Xantheas, S. S. *J. Am. Chem. Soc.* **1995**, *117*, 10373.
(50) Pudzianowski, A. T. *J. Chem. Phys.* **1995**, *102*, 8029.
(51) Hannachi, Y.; Silvi, B.; Bouteiller, Y. *J. Chem. Phys.* **1991**, *94*, 2915.
(52) Markovich, G.; Pollak, S.; Giniger, R.; Cheshnovsky O. *J. Chem. Phys.* **1994** *101*, 9345.
(53) Combariza, J. E.; Kestner, N. R.; Jortner, J. *J. Chem. Phys.* **1994**, *100*, 2851.
(54) Note that our model prevents any energy flow into vibrational degrees of freedom of the solvent. However, a previous simulation study of a similar reactive process in flexible water confirms the absence of any relevant energy dissipation into intramolecular degrees of freedom of the bath. See: Gertner, B. J.; Whitnell, R. M.; Wilson, K. R.; Hynes, J. T. *J. Am. Chem. Soc.* **1991**, *113*, 74.
(55) Maroncelli, M. *J. Mol. Liq.* **1993**, *57*, 1.
(56) See, for example: Chandler, D. *Introduction to Modern Statistical Mechanics;* Oxford University Press: New York, 1987; Chapter 8.
(57) Maroncelli, M.; Fleming, G. R. *J. Chem. Phys.* **1988**, *89*, 5044.
(58) Re, M.; Laria, D. *J. Phys. Chem. B* **1997**, *101*, 10494.
(59) Miura, S.; Tuckerman, M. E.; Klein, M. L. *J. Chem. Phys.* **1998**, *109*, 5290.